A Late Archean Sulfidic Sea Stimulated by Early Oxidative Weathering of the Continents

Christopher T. Reinhard,[1] Rob Raiswell,[2] Clint Scott,[1] Ariel D. Anbar,[3] Timothy W. Lyons[1]*

Iron speciation data for the late Archean Mount McRae Shale provide evidence for a euxinic (anoxic and sulfidic) water column 2.5 billion years ago. Sulfur isotope data compiled from the same stratigraphic section suggest that euxinic conditions were stimulated by an increase in oceanic sulfate concentrations resulting from weathering of continental sulfide minerals exposed to an atmosphere with trace amounts of photosynthetically produced oxygen. Variability in local organic matter flux likely confined euxinic conditions to midportions of the water column on the basin margin. These findings indicate that euxinic conditions may have been common on a variety of spatial and temporal scales both before and immediately after the Paleoproterozoic rise in atmospheric oxygen, hinting at previously unexplored texture and variability in deep ocean chemistry during Earth's early history.

The first two billion years of Earth's history were characterized by little to no free atmospheric oxygen (*1*, *2*). A large body of evidence points to a sharp rise in the concentration of atmospheric O_2 during the Paleoproterozoic between 2.45 and 2.32 billion years ago (Ga) (*1*–*3*), but the history of deep ocean oxygenation is less well-known. The deposition of banded iron formations (BIF) during the Archean and early Proterozoic (~3.8 to 1.8 Ga) has been taken to imply that deep ocean water masses were anoxic and rich in dissolved ferrous iron (Fe^{2+}) derived from high-temperature weathering of seafloor basalt under low oceanic sulfate (SO_4^{2-}) concentrations (*4*, *5*). Reducing and iron-rich (ferruginous) deep ocean conditions are thought to have persisted for most of Earth's early history, although a relative paucity of BIF between 2.4 and 2.0 Ga (*6*) has rendered deep ocean chemistry during this period obscure. In any case, the cessation of BIF deposition at ~1.8 Ga is generally linked to the accumulation of oxygen in the atmosphere through the eventual removal of Fe^{2+} from the ocean either as ferric (hydr)oxides (*7*) or as pyrite in euxinic basins (*8*). A corollary of the latter model is that oxidative delivery of sulfate to the ocean was not sufficient to remove reactive iron through microbial sulfide production before ~1.8 Ga. However, recent studies of the late Archean Mount McRae Shale suggest that oxidative sulfur cycling may have preceded the Paleoproterozoic rise in atmospheric oxygen (*9*) and that conditions sufficient to authigenically enrich molybdenum (Mo) in marine sediments existed at ~2.5 Ga (*10*). On the modern Earth, substantial enrichment of Mo into sediments occurs after the conversion of soluble molybdate (MoO_4^{2-}) to particle-reactive thiomolybdates ($MoO_{4-x}S_x^{2-}$) in stable sulfidic environments (*11*), indicating that the Mo enrichments seen in the Mount McRae Shale may have resulted from the development of a euxinic water column in association with increased oxidative transport of crustal sulfur as SO_4^{2-}.

To examine the possibility of euxinia during the late Archean, we analyzed iron mineral speciation in the Mount McRae Shale (*12*). The distribution of iron among different biogeochemically labile mineral phases ("highly reactive iron") can reveal local redox conditions (*13*, *14*). Highly reactive iron (Fe_{HR}) is defined as the sum of pyrite iron (Fe_{PY}) and iron in phases that are reactive to hydrogen sulfide (H_2S) on short diagenetic time scales, such as ferric oxides (Fe_{ox}), magnetite (Fe_{mag}), and iron present as carbonate (Fe_{carb}). In modern sediments from oxic continental margins and the deep sea, Fe_{HR} makes up 6 to 38% of the total sedimentary iron (Fe_T) (i.e., Fe_{HR}/Fe_T = 0.06 to 0.38); an average Fe_{HR}/Fe_T ratio of 0.26 ± 0.08 defines the modern siliciclastic baseline (*13*). Values for Fe_{HR}/Fe_T that are elevated above this siliciclastic background suggest reactive iron input that is decoupled from detrital sources, an indication of iron transport and scavenging within an anoxic water column (*15*). We also look toward total iron enrichments (expressed as Fe_T/Al ratios) as an indicator of water column anoxia (*16*, *17*).

If Fe_{HR}/Fe_T and Fe_T/Al data provide evidence for anoxia, the ratio Fe_{PY}/Fe_{HR} can be used to distinguish between anoxic but nonsulfidic conditions and anoxic water columns containing free H_2S (euxinic). This approach is based on the simple premise that under anoxic conditions dissolved Fe^{2+} and dissolved H_2S cannot coexist in abundance in solution because of the insolubility of iron sulfide phases, and therefore high values for Fe_{PY}/Fe_{HR} indicate H_2S-dominated water column chemistry. For confirmation, we also measured degree of pyritization (DOP) as a conservative indicator of iron-limited pyrite formation and euxinia (*12*, *17*). The distribution of highly reactive Fe species in the Mount McRae Shale is shown in Fig. 1, along with Fe_T/Al, bulk molybdenum (Mo), and organic carbon (TOC) concentrations from (*10*). We focus here on the pyritic and organic-rich lower shale interval (LSI) and upper shale interval (USI). Ferric oxides make up a small proportion of Fe_{HR} for the entire sequence analyzed here, indicating water column and/or pore fluid conditions that were reducing with respect to iron (Fig. 1). Values for Fe_{HR}/Fe_T and Fe_T/Al are elevated throughout, suggesting that the entire sequence was deposited beneath an anoxic water column. In a few instances, Fe_{PY}/Fe_{HR} values in the LSI approach a threshold ($Fe_{PY}/Fe_{HR} \geq 0.8$) interpreted to reflect euxinia when paired with evidence for anoxic deposition (*14*, *18*); however, the average Fe_{PY}/Fe_{HR} for this unit (0.55 ± 0.20) suggests a predominance of ferruginous conditions. Variations in Fe_{HR} within the LSI are governed by differences in Fe_{carb} rather than Fe_{PY} (fig. S2). These data are consistent with sulfate reduction and pyrite formation within or beneath an anoxic water column, but with reactive Fe in excess of dissolved H_2S such that H_2S did not persist in the pore fluids or water column during LSI deposition.

The USI shows pronounced enrichment in Fe_{HR}, indicating extensive reactive Fe scavenging beneath an anoxic water column (Fig. 1). Values for Fe_T/Al, although lower than those seen in the underlying siderite-facies, remain elevated. In contrast to the LSI, Fe_{PY}/Fe_{HR} values are persistently high (0.85 ± 0.17), as is DOP (0.78 ± 0.23). A strong linear relation between Fe_{HR} and Fe_{PY} for the USI (fig. S2) demonstrates that variations in the amount of Fe_{HR} are governed by differences in Fe_{PY} content and that Fe_{HR} is all but completely pyritized. This combination of parameters (elevated values for Fe_{HR}/Fe_T, Fe_T/Al, Fe_{PY}/Fe_{HR}, and DOP) indicates that the water column was euxinic for a substantial portion of USI deposition.

To examine whether euxinia occurred in association with a transient or secular change in the oxidative transport of MoO_4^{2-} and SO_4^{2-} (*19*), we turn to the sulfur isotope composition of syngenetic and early diagenetic pyrite from deep-water facies (shales and BIF) of the Neoarchean-Paleoproterozoic (2.7 to 2.45 Ga) Hamersley Basin (Fig. 2). Neoarchean samples below the USI, including those from the LSI and the siderite-facies BIF directly beneath the USI, show large $\Delta^{33}S$ values and positive covariation between $\Delta^{33}S$ and $\delta^{34}S$ (Fig. 2). This pattern has been hypothesized to reflect a primary atmospheric array in the isotopic composition of elemental sulfur aerosols (*20*). The corresponding linearity and large positive $\Delta^{33}S$ anomalies of these data suggest a tight isotopic coupling between atmospherically derived reduced sulfur species and sedimentary pyrite formation and also indicate that the transfer and mixing mechanisms that contributed to the signal ultimately preserved in the sediments were similar on at

[1]University of California–Riverside, Department of Earth Sciences, Riverside, CA 92521, USA. [2]University of Leeds, School of Earth and Environment, Leeds, UK LS2 9JT. [3]Arizona State University, School of Earth and Space Exploration and Department of Chemistry and Biochemistry, Tempe, AZ 85287, USA.

*To whom correspondence should be addressed. E-mail: timothyl@ucr.edu

least a basinal scale and through large periods of Archean time (*9*, *20*).

The sulfur isotope composition of pyrite in the USI and the overlying Brockman BIF shows a different distribution (Fig. 2). Values for $\Delta^{33}S$ are attenuated during euxinic deposition, with the largest positive $\Delta^{33}S$ values in the USI found in intervals that are transitional with the siderite-facies BIF unit below or the overlying carbonate unit. The linear array that characterizes the data before deposition of the USI is no longer evident, and a linear regression through the USI/Brockman data is closely aligned with the mass-dependent fractionation array in $\delta^{34}S$-$\delta^{33}S$ space. This shift is accompanied by predominantly small negative $\Delta^{33}S$ values and relatively depleted $\delta^{34}S$ values within the USI, followed by subdued variability in $\Delta^{33}S$ and a wide spread in $\delta^{34}S$ values [from –5 per mil (‰) to +35‰] in the overlying Brockman BIF. We interpret this isotopic shift to reflect increased SO_4^{2-} availability during deposition of the USI and Brockman BIF accompanied by mixing of photolytically produced sulfur and isotopically normal crustal sulfur oxidatively mobilized under an atmosphere that remained O_2-poor (*12*). A transient or secular increase in the oxidative transport of MoO_4^{2-} and SO_4^{2-} during USI deposition is also supported by the contrasting strong non–mass-dependent (NMD) signal (*20*) and essential lack of Mo enrichment (*21*) preserved in pyritic shales of the Jeerinah Formation underlying the Mount McRae—analogous to the signals seen in the LSI and the siderite-facies BIF beneath the USI. The persistence of distinct NMD anomalies, despite the overall shift in isotopic arrays, requires the formation and burial of sulfur with NMD isotope composition throughout this period. Ground-level atmospheric O_2 concentrations of less than 2 parts per million by volume (ppmv) (i.e., below 10^{-5} the present atmospheric level) are therefore implied (*22*), and concentrations throughout most of the troposphere may have been substantially lower than this (*22*, *23*). This assertion is also supported by $\Delta^{33}S/\Delta^{36}S$ relationships (*9*).

Combined, the high-resolution Fe speciation, Mo enrichment, and sulfur isotope data for the Mount McRae Shale indicate the development of euxinia during deposition of the USI and that these conditions were contemporaneous with a change in sedimentary sulfur isotope systematics. However, the stratigraphic position of the USI between two BIFs, coupled with Fe_T/Al ratios that are persistently and substantially elevated above crustal values (Fig. 1), suggest that hydrothermal iron fluxes to the deep basin were important at this time. Our interpretation therefore implies a water column structure that would allow for both the accumulation of dissolved H_2S and the subsequent or coeval deposition of voluminous BIF.

To reconcile these observations, we postulate locally enhanced microbial H_2S production, stimulated by organic matter (OM) delivery and facilitated by an increased flux of dissolved SO_4^{2-} to the basin. Local loading of OM would have fueled vigorous sulfate reduction along the basin margin, resulting in an oxidant minimum zone in which dissolved H_2S accumulated and quantitatively removed dissolved Fe^{2+} from the water column (Fig. 3). Euxinia would have expanded or contracted periodically as a function of the balance between reactive Fe input and OM flux, with the possibility of dissolved H_2S transiently accumulating on a basin scale or receding beneath the sediment-water interface. This lateral redox structure is similar to the basin-scale lithofacies framework hypothesized for contemporaneous strata from the South African Transvaal basin (*24*), indicating that such conditions may have been common during this period.

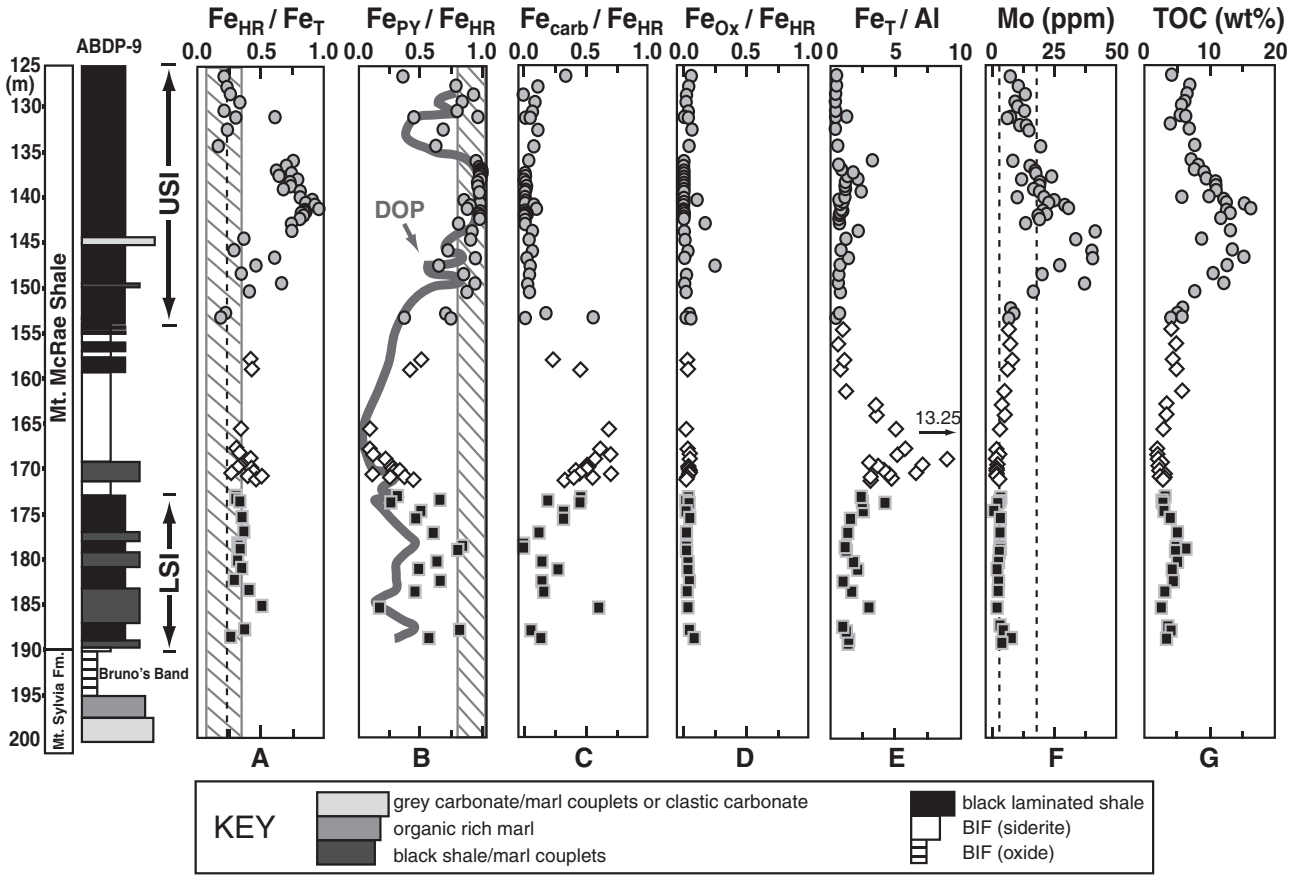

Fig. 1. (**A** to **G**) Stratigraphic profiles for iron speciation data from the ADBP-9 core. Squares, diamonds, and circles represent the LSI, siderite-facies BIF, and USI, respectively. The striped box in (A) represents the range of Fe_{HR}/Fe_T values seen in modern oxic continental margin and deep-sea sediments (*13*). The dotted line in (A) represents the mean Fe_{HR}/Fe_T value (0.26) for normal (oxic) marine settings (*13*). The striped box in (B) represents Fe_{PY}/Fe_{HR} values that are above 0.8. Euxinia is implied when both of these thresholds are exceeded and Fe_T/Al values exceed 0.5. The dark line in (B) is the best fit through DOP values (not shown). The two dotted lines in (E) reflect average bulk Mo enrichments for the Archean [3 parts per million (ppm)] and Proterozoic (18 ppm) (*21*). Data for (E) and (F) from (*10*).

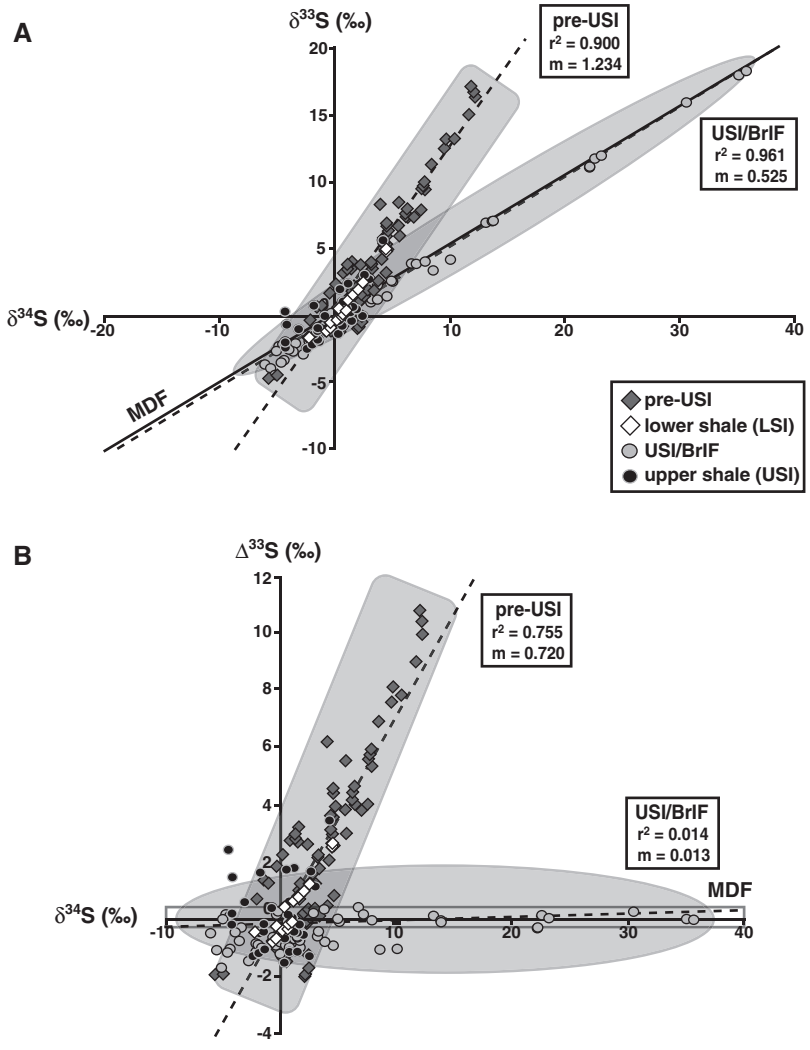

Fig. 2. Sulfur isotope data for deep-water Hamersley Basin pyrite samples spanning 2.7 to 2.45 Ga, displayed as $\delta^{34}S$ versus $\delta^{33}S$ (**A**) and $\delta^{34}S$ versus $\Delta^{33}S$ (**B**). Pre-USI data are from the Jeerinah Formation and lower Mount McRae Shale (*20*, *27*); the LSI and siderite-facies BIF beneath the USI (*9*); and the Marra Mamba BIF (*27*), which was deposited between the Jeerinah Formation and the Mount McRae Shale. USI/Brockman BIF (BrIF) data are from the USI (*9*) and the overlying BrIF (*27*, *28*). The line labeled "MDF" in (A) is the mass-dependent fractionation line, defined as $\delta^{33}S = 0.515 \times \delta^{34}S$ (*29*). The gray box in (B) represents the range of $\Delta^{33}S$ values attainable by mass-dependent processes (*30*, *31*).

Although OM delivery was the proximate cause of euxinia, we propose that it was the increased availability of SO_4^{2-} attendant to oxidative weathering that ultimately allowed microbial H_2S production to overwhelm reactive Fe, at least locally, during USI deposition. Elevated total sulfur concentrations in this interval, coincident with increased TOC and high Fe_T values (*9*, *10*), also point to increasing availability of water column SO_4^{2-} such that microbial sulfate reduction was able to keep pace with substantial OM flux and relatively high reactive Fe availability. It is possible that mid-water column euxinia existed subsequent to USI deposition, with the stratigraphic transition to Brockman BIF recording a change in water depth rather than a temporal change in basin chemistry.

Our findings suggest that weak oxidative forcing could have stimulated the development of euxinia 50 to 100 million years before the Paleoproterozoic rise in atmospheric oxygen and that stable and persistent euxinia could have developed at least locally, and perhaps on a much larger scale, even within BIF-forming basins. Sulfur isotope data indicate that the weathering flux of SO_4^{2-} to the ocean increased substantially after the rise in atmospheric oxygen between 2.45 and 2.32 Ga (*8*, *25*). The lack of BIF between 2.4 and 2.0 Ga may therefore reflect the frequent or sustained development of euxinia within Paleoproterozoic basins (*1*), presaging the possibly widespread and protracted development of similar oceanographic conditions hypothesized previously for the Mesoproterozoic (~1.8 to 1.0 Ga) (*8*). Constraints on deep ocean redox during this intervening period are sparse, but existing data intimate that euxinic deep basins were much more common than ferruginous ones between 2.4 and 2.0 Ga (*21*).

More generally, we argue that deposition of BIFs represented episodic pulses of reducing power from Earth's interior (*6*) rather than persistent deep-water conditions. Significant spatial variability in water column chemistry is indicated for intervals of BIF deposition, with intervening periods throughout the Archean and Paleoproterozoic during which at least portions of the water column may have been euxinic. Vacillation be-

Fig. 3. Schematic representation of the Hamersley Basin during the deposition of the upper Mount McRae Shale (USI). Oxidative delivery of SO_4^{2-} and MoO_4^{2-}, combined with a high local organic matter flux, resulted in the accumulation of free H_2S in the water column in excess of dissolved Fe^{2+} (euxinia), supporting authigenic Mo enrichment. Atmospheric O_2 concentrations below 2 ppmv could have driven the enhanced oxidative weathering recorded in the USI but would still have allowed for SO_2 photolysis and the preservation of NMD sulfur isotope anomalies (*12*). Atmospheric photochemistry simplified from (*32*).

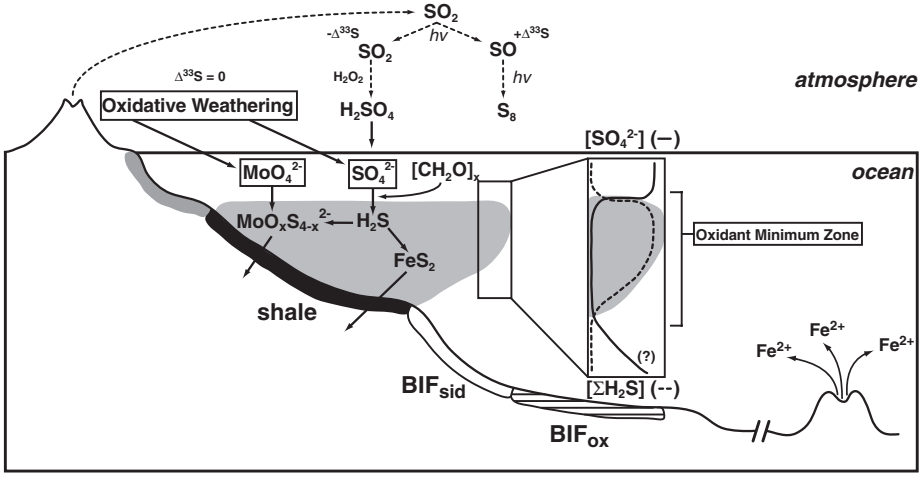

tween euxinic and ferruginous conditions would have favored the early evolution and ecological expansion of a variety of anoxygenic photosynthetic metabolisms in pelagic environments. Expressions of biological oxygen production (such as those seen in the upper Mount McRae and Brockman BIF) would then have varied with the extent to which episodic or sustained pulses of reductants from the Earth's interior would have buffered photosynthetic oxygen, contributing to the protracted nature of Earth surface oxygenation during the Archean and Proterozoic (*26*).

References and Notes

1. D. E. Canfield, *Annu. Rev. Earth Planet. Sci.* **33**, 1 (2005).
2. H. D. Holland, *Geochim. Cosmochim. Acta* **66**, 3811 (2002).
3. A. Bekker *et al.*, *Nature* **427**, 117 (2004).
4. A. E. Isley, *J. Geol.* **103**, 169 (1995).
5. L. R. Kump, W. E. Seyfried, *Earth Planet. Sci. Lett.* **235**, 654 (2005).
6. A. E. Isley, D. H. Abbott, *J. Geophys. Res.* **104**, 15461 (1999).
7. P. E. Cloud, *Am. J. Sci.* **272**, 537 (1972).
8. D. E. Canfield, *Nature* **396**, 450 (1998).
9. A. J. Kaufman *et al.*, *Science* **317**, 1900 (2007).
10. A. D. Anbar *et al.*, *Science* **317**, 1903 (2007).
11. B. E. Erickson, G. R. Helz, *Geochim. Cosmochim. Acta* **64**, 1149 (2000).
12. Materials and methods are available as supporting material on *Science* Online.
13. R. Raiswell, D. E. Canfield, *Am. J. Sci.* **298**, 219 (1998).
14. S. W. Poulton, P. W. Fralick, D. E. Canfield, *Nature* **431**, 173 (2004).
15. J. W. M. Wijsman, J. J. Middelburg, C. H. R. Heip, *Mar. Geol.* **172**, 167 (2001).
16. Interpretation of this measurement follows the same rationale as that for Fe_{HR}/Fe_T (i.e., enrichments above the average Fe_T/Al ratio for continental crust of ~0.5 imply transport and scavenging of iron under anoxic conditions), but Fe_T/Al is immune to concerns regarding authigenic iron-silicate formation or metamorphic repartitioning of reactive iron phases into poorly reactive silicate mineralogies.
17. T. W. Lyons, S. Severmann, *Geochim. Cosmochim. Acta* **70**, 5698 (2006).
18. T. F. Anderson, R. Raiswell, *Am. J. Sci.* **304**, 203 (2004).
19. Because Mo enrichments require both an oceanic Mo reservoir and the accumulation of free H_2S, it is possible that the metal enrichments recorded in the USI point only to the development of euxinia rather than a temporally constrained increase in the flux of MoO_4^{2-} and SO_4^{2-} to the Hamersley Basin during USI deposition.
20. S. Ono *et al.*, *Earth Planet. Sci. Lett.* **213**, 15 (2003).
21. C. Scott *et al.*, *Nature* **452**, 456 (2008).
22. A. A. Pavlov, J. F. Kasting, *Astrobiology* **2**, 27 (2002).
23. K. Zahnle, M. Claire, D. Catling, *Geobiology* **4**, 271 (2006).
24. C. Klein, N. J. Beukes, *Econ. Geol.* **84**, 1733 (1989).
25. E. M. Cameron, *Nature* **296**, 145 (1982).
26. L. R. Kump, M. E. Barley, *Nature* **448**, 1033 (2007).
27. M. Partridge, S. D. Golding, K. A. Baublys, E. Young, *Earth Planet. Sci. Lett.* (2008).
28. S. J. Mojzsis, C. D. Coath, J. P. Greenwood, K. D. McKeegan, T. M. Harrison, *Geochim. Cosmochim. Acta* **67**, 1635 (2003).
29. J. R. Hulston, H. G. Thode, *J. Geophys. Res.* **70**, 3475 (1965).
30. J. Farquhar *et al.*, *Geobiology* **1**, 27 (2003).
31. S. Ono, B. Wing, D. Johnston, J. Farquhar, D. Rumble, *Geochim. Cosmochim. Acta* **70**, 2238 (2006).
32. J. F. Kasting, K. J. Zahnle, J. P. Pinto, A. T. Young, *Orig. Life Evol. Biosph.* **19**, 95 (1989).

33. The NASA Astrobiology Institute and Exobiology Program and the NSF Geobiology and Low Temperature Geochemistry Program provided financial support. The authors thank B. Gill, S. Severmann, N. Planavsky, M. Claire, J. Kaufman, and R. Buick for helpful discussions, and G. Arnold for handling of core material.

Supporting Online Material

www.sciencemag.org/cgi/content/full/326/5953/713/DC1
Materials and Methods
Figs. S1 to S3
Table S1
References

22 May 2009; accepted 31 August 2009
10.1126/science.1176711

Improved Attribution of Climate Forcing to Emissions

Drew T. Shindell,* Greg Faluvegi, Dorothy M. Koch, Gavin A. Schmidt, Nadine Unger, Susanne E. Bauer

Evaluating multicomponent climate change mitigation strategies requires knowledge of the diverse direct and indirect effects of emissions. Methane, ozone, and aerosols are linked through atmospheric chemistry so that emissions of a single pollutant can affect several species. We calculated atmospheric composition changes, historical radiative forcing, and forcing per unit of emission due to aerosol and tropospheric ozone precursor emissions in a coupled composition-climate model. We found that gas-aerosol interactions substantially alter the relative importance of the various emissions. In particular, methane emissions have a larger impact than that used in current carbon-trading schemes or in the Kyoto Protocol. Thus, assessments of multigas mitigation policies, as well as any separate efforts to mitigate warming from short-lived pollutants, should include gas-aerosol interactions.

Multicomponent climate change mitigation strategies are likely to be much more cost effective than carbon dioxide (CO_2)–only strategies (*1*, *2*) but require quantification of the relative impact of different emissions that affect climate. Because globally and annually averaged radiative forcing (RF) is generally a good predictor of global mean surface temperature change, a scale related to RF is a logical choice for comparing emissions. The most widely used, and that adopted in the Kyoto Protocol, is the global warming potential (GWP), defined as the integrated global mean RF out to a chosen time of an emission pulse of 1 kg of a compound relative to that for 1 kg of CO_2. GWPs are thus based on radiative impact and atmospheric residence time and can include both the direct radiative effect of emitted species and radiative effects from indirect chemical responses. Previous studies, including the Intergovernmental Panel on Climate Change (IPCC) Fourth Assessment Report (AR4), provide estimates of RF and GWPs of short-lived gas emissions (*3*–*5*). However, except for the indirect effect of NO_x emissions on nitrate aerosol, gas-aerosol interactions were not included. These interactions occur primarily through ozone precursors altering the availability of oxidants, influencing aerosol formation rates, and through sulfate-nitrate competition for ammonium.

We used the composition-climate model Goddard Institute for Space Studies (GISS) Model for Physical Understanding of Composition-Climate Interactions and Impacts (G-PUCCINI) (*6*) to calculate the response to removal of all anthropogenic methane, carbon monoxide (CO) plus volatile organic compounds (VOCs), NO_x, SO_2, and ammonia emissions. This model couples gas-phase, sulfate (*7*), and nitrate (*8*) aerosol chemistry within the GISS ModelE general circulation model (GCM). Anthropogenic emissions are from a 2000 inventory (*9*). We calculated both the "abundance-based" RF owing to the net atmospheric composition response by species when all emissions are changed simultaneously and the "emissions-based" forcing attributable to the responses of all species to emissions of a single pollutant (Fig. 1). The sum of the forcings that take place via response of a particular species in the emissions-based analysis (each represented by a different color in Fig. 1) is approximately equal to the forcing due to that species in the abundance-based analysis. Likewise, the sums of all emissions-based and all abundance-based forcings are similar. Hence, the two viewpoints provide different but compatible pictures of how emissions and composition changes influence RF.

Emissions of NO_x, CO, and methane have substantial impacts on aerosols by altering the abundance of oxidants, especially hydroxyl, which convert SO_2 into sulfate. Global burdens of hydroxyl and sulfate change by 18% and 13% for increased NO_x, by –13% and –9% for CO, and by –26% and –11% for methane (sulfate forcing closely follows the sulfate burden change). Coupling in the other direction is very weak because reactions of gas-phase species upon aerosol surfaces have only a small effect on the global burden of the radiatively active species ozone and methane (e.g., anthropogenic SO_2 emissions enhance the removal of NO_x through reactions on particulate

NASA Goddard Institute for Space Studies and Columbia University, New York, NY 10025, USA.

*To whom correspondence should be addressed. E-mail: drew.t.shindell@nasa.gov

Science

A Late Archean Sulfidic Sea Stimulated by Early Oxidative Weathering of the Continents

Christopher T. Reinhard, Rob Raiswell, Clint Scott, Ariel D. Anbar and Timothy W. Lyons

Science **326** (5953), 713-716.
DOI: 10.1126/science.1176711

Of Ancient Iron and Oxygen

Finding clues to understand the early evolution of ocean and atmospheric chemistry and its links to the evolution of life remains a daunting task. Often just a few rock samples provide our only evidence of what conditions on Earth were like long ago. **Reinhard *et al.*** (p. 713) combined iron speciation data from a 2.5-billion-year-old shale from Australia with sulfur isotope data from this and nearby formations to conclude that oxygen chemistry predominanty consisted of an anoxic sulfide–rich water column, instead of iron-rich oceans, as previously speculated. Thus, brief pulses of reduced iron from hydrothermal vents may have been responsible for the formation of nearby banded iron formations and may have provided enough buffering to prolong the appearance of atmospheric oxygen generated by the expansion of newly evolved cyanobacteria.